

Isotope effect and electron-temperature dependence in volume H^- and D^- ion sources

D. A. Skinner,* A. M. Bruneteau, P. Berlemont, C. Courteille, R. Leroy, and M. Bacal

Laboratoire de Physique des Milieux Ionisés, Laboratoire du CNRS, Ecole Polytechnique, 91128 Palaiseau Cedex, France

(Received 19 April 1993)

We present the results of a numerical study of isotope effects in volume negative-ion sources and compare them with experimental results. We have studied both hydrogen and deuterium discharges over a range of discharge current. For basic plasma parameters, the model reproduces the behavior measured in the discharge region of a tandem multicusp source. The theory predicts a local maximum in negative-ion production at an optimal electron temperature $T_e^{\text{opt}} \approx 0.6\text{--}0.8$ eV. This prediction is supported by our analysis of D^- and H^- densities measured in a hybrid multicusp source and in the extraction region of a tandem source. We show how the local maximum is related to the temperature dependence of the dissociative attachment rate coefficients. The most significant isotope effect suggested by this modeling effort is a stronger cooling of the vibrational distribution in deuterium due to vibration-translation reactions between molecules and atoms. This vibrational cooling reduces negative-ion production in high-power deuterium discharges below that in equivalent hydrogen discharges.

PACS number(s): 52.80.Sm, 29.25.Ni, 52.20.-j, 33.10.Gx

I. INTRODUCTION

Much effort has been dedicated in the past decade to the development of neutral-particle beams based on the neutralization of high-energy hydrogen negative-ion beams [1,2]. One of the most important uses for high-energy neutral-particle beams is controlled thermonuclear fusion research. This and other applications call for the use of D^- -ion beams rather than beams of the lighter isotope. Therefore there is much interest in the isotope scaling of the negative-ion production in negative-ion sources. One of the ion sources considered for these applications is the volume ion source [3,4] in which the negative ions are produced in a low-pressure discharge in pure hydrogen or deuterium. It is generally admitted that the process responsible for the negative-ion production in these sources is dissociative attachment of electrons to rovibrationally excited molecules [4,5]. Modeling of the multicusp hydrogen discharges has been effected and its results compared with measured H_2 vibrational distributions [6–11]. Quantitative agreement was found for the general plasma properties (electron density and temperature, atomic density, the vibrationally excited populations of levels $v''=0\text{--}4$); discrepancies remain in the prediction of the vibrationally excited molecular populations with $v'' > 4$ and of the negative-ion density.

Most of the experimental investigations have concentrated on the study of hydrogen discharges. Recently attempts were made to investigate the isotope scaling of volume negative-ion sources based essentially on the measurement of the extracted negative-ion and electron beams [12–16] associated in some cases [12–14] with a limited knowledge of the plasma properties. As a result, it appeared that the isotope scaling depends on the source design while the differences among the various observations are still to be explained. Measurements of the isotope effect on negative-ion density have now been made using photodetachment techniques in a hybrid multicusp

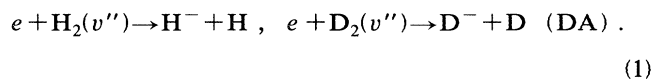
source [17,18] and a tandem source [19].

The present work has three principal goals: (1) to apply our numerical model of the multicusp discharge to the case of a discharge in deuterium, and compare the results with modeling an identical discharge operated in hydrogen; (2) to study the dependence of negative-ion production on electron temperature where negative ions are produced; and (3) to verify the extent to which the general predictions of this theoretical effort are consistent with experimental results, especially photodetachment measurements of negative-ion density.

Our basic numerical model and its application to deuterium are described in Sec. II. The isotope effect on basic plasma parameters predicted by the numerical model is presented in Sec. III and compared with experimental data. Section IV discusses the isotope effect predicted for the vibrational spectrum and negative-ion production. *In situ* measurements of H^- and D^- density in a hybrid source will be presented and analyzed in Sec. V. Photodetachment measurements comparing H^- and D^- densities have recently become available in a tandem source also, and they will be discussed in Sec. VI. The negative-ion density measurements will be compared to theoretical predictions in Sec. VII.

II. THE THEORETICAL MODEL OF VOLUME NEGATIVE-ION PRODUCTION

The negative ions are thought to be produced in volume sources through dissociative attachment (DA) of electrons to vibrationally excited molecules [5]:



Several reactions have been considered for the production and quenching of the vibrationally excited molecules. They have been discussed in detail in numerous publications (e.g., Ref. [4]). Electron-molecule collisions, atom-

molecule, and molecule- and atom-surface collisions are important in shaping the vibrational spectrum of the molecules. Table I lists the most important reactions, based on information gained by studying hydrogen sources. We assume that these reactions are relevant to simulating a discharge in deuterium as well. For the most important processes in an existing code for hydrogen [6,9,20–23], we have substituted cross sections and rate constants for deuterium.

One of the difficulties in modeling this type of discharge is the fact that wall collisions of atoms and molecules are important while their interaction with the surface under plasma conditions is not sufficiently understood. The atomic density is inversely proportional to the recombination probability of atoms on surfaces γ_H . This factor depends on experimental conditions, such as the wall temperature and the degree of contamination of the wall surface by material evaporated from the filaments. In modeling this factor is adjusted to fit the atomic density, when experimental data are available.

The problem of modeling hydrogen-atom- and -molecule-surface interactions is also present for deuterium, but even less information is available for deuterium than for hydrogen. Our approach has been to choose for this study a large plasma source, operated at relatively high power, where vibrational cooling in molecule-wall

collisions is relatively unimportant. We estimated vibrational wall quenching in deuterium by using the same model for de-excitation probability (as a function of initial and final vibrational level) employed for hydrogen.

A simple model is used for atomic wall recombination: (a) we assumed equal atomic temperatures, meaning that the wall collision rate in deuterium is lowered by a factor of $1/\sqrt{2}$; and (b) we used a deuterium-wall recombination probability γ_D equal to that adopted for hydrogen [6,20] $\gamma_H=0.05$. A recent theoretical study [24] of atomic recombination on a copper surface indicates that the reaction probabilities for H and D are equal and have a similar behavior. This supports the simple assumption $\gamma_D=\gamma_H$, which we made in the model, although we attributed much lower values than found in Ref. [24]. However, if cross-surface diffusion of atoms were important in atomic recombination via the Langmuir-Hinshelwood mechanism, then the lower mobility of surface-adsorbed D would suggest $\gamma_D < \gamma_H$. This possibility receives some support from measurements in a multipole discharge [25] which found the atomic density ratio n_D/n_H to be higher than what would be expected from a $\sqrt{2}$ scaling law.

Atoms play a major role in cooling the vibrational distribution, especially at high discharge current, through vibration-translation (V-T) collisions. For V-T collisions

TABLE I. Reactions in the model involving heavy species: vibrational excitation of D_2 by collisions with low- and high-energy electrons e-V and E-V); cooling of vibrationally excited $D_2(v'')$ by wall collisions (wall), by vibration-translation reactions with atoms and molecules (V-t and V-T), and by vibration-vibration reactions (V-V); ionization of atoms and molecules (IZ-a and IZ-m); wall recombination of atoms (ra); a model of ion losses consisting of ion-molecule reaction (IM), wall recombination (ri), and dissociative recombination (DR); D^- creation by dissociative attachment (DA); D^- destruction by mutual neutralization (MN), electron detachment (ED), and associative detachment (AD). The computational model includes all reactants and products of each reaction. For some reactions the hydrogen rate constants or cross sections were retained for the deuterium modeling, either because a reaction is relatively unimportant, because it has no isotope dependence, or because its isotope dependence is unknown.

Label	Reaction	Modifications for D
e-V	$e + D_2(v) \rightarrow e + D_2(v'')$	from Refs. [5] and [30]
E-V	$e + D_2(v=0) \rightarrow e + D_2^*(B^1\Sigma_u^+, C^1\Pi_u) \rightarrow e + D_2(v'') + h\nu$	New calculations for H and D, Refs. [27] and [32]
Wall	$D_2(v'') + \text{wall} \rightarrow D_2(v), v < v''$	none (see text)
V-t	$D_2(v'') + D \rightarrow D_2(v) + D, v < v''$	Ref. [29] (see text)
V-T	$D_2(v'') + D_2(v') \rightarrow D_2(v''-1) + D_2(v')$	none
V-V	$D_2(v'') + D_2(v') \rightarrow D_2(v''-1) + D_2(v'+1)$	none
DS	$D_2(v'') + e \rightarrow e + D_2^*(b^3\Sigma_u^+, c^3\Pi_u, ^3\Sigma_g^+) \rightarrow e + 2H$	new $D_2^*(b^3\Sigma_u^+, c^3\Pi_u)$ from Ref. [32]
IZ-a	$D + e \rightarrow D^+ + 2e$	none
IZ-m	$D_2(v'') + e \rightarrow D_2^+ + 2e$	from Ref. [32]
ra	$D + D(\text{wall}) \rightarrow D_2(v'')$	same γ and atomic T
IM	$D_2(v'') + D_2^+ \rightarrow D_3^+ + D$	$1/\sqrt{2}$ (see text)
ri	$D_n^+ + e(\text{wall}) \rightarrow \text{neutral species}$	$1/\sqrt{2}$ and same ion T
DR	$D_n^+ + e(\text{volume}) \rightarrow \text{neutral species}$	none
DA	$D_2(v'') + e \rightarrow D + D^-$	Refs. [5,30,31] (see text)
MN	$D^- + D_n^+ \rightarrow \text{neutral species}$	none (see text)
ED	$D^- + e \rightarrow D + 2e$	none
AD	$D^- + D \rightarrow D_2(v'') + e$	none (see text)

with atoms, we use rate constants based on the Monte Carlo calculations of Laganà and co-workers [26–29] for atomic and molecular temperatures of 4000 and 500 K, respectively. For hydrogen, we use polynomial fits (as functions of initial and final vibrational levels) to Laganà's data provided by Gorse [28]. For deuterium, we use our own polynomial fits to Laganà's data [29] of lower order and incorporating more smoothing than was the case for hydrogen, since there is more statistical noise in the deuterium data.

Positive ions are principally destroyed by transport to the walls where they are neutralized. For deuterium, we took this transport to be a factor $1/\sqrt{2}$ smaller than for hydrogen, from the square root of the mass ratio. In the absence of specific information, perhaps the simplest isotope scaling follows from the ansatz of an isotope-independent constant cross section (e.g., hard-sphere collisions). A rate constant $\langle\sigma v\rangle$ would then vary with the mean center-of-mass velocity. If we assume the same temperatures in hydrogen and deuterium discharges, then in deuterium the slower thermal speeds would lower $\langle\sigma v\rangle$ by the factor $1/\sqrt{2}$ in comparison with hydrogen. We have adopted this $1/\sqrt{2}$ scaling for the ion-molecule reaction $D_2 + D_2^+ \rightarrow D + D_3^+$, denoted IM in Table I. We defer discussion of the negative-ion destruction processes of associative detachment (AD) and mutual neutralization (MN) to the end of Sec. IV.

For cross sections relevant to electronic processes, we use, when available, cross sections for hydrogen and deuterium obtained using the same method. Since the electronic structure of the two isotopes is very similar, only a limited number of cross sections are expected to be different because of the difference in vibrational structure. An example of a reaction with isotope-dependent cross section is dissociative attachment [Eq. (1)]. In this case we use the cross sections calculated by Bardsley and Wadehra [5,30] for the rotational state $J=1$. These calculations also provided the cross sections for the vibrational excitation due to low-energy electrons, denoted e-V in Table I. However, in the case of hydrogen these theoretical cross sections have been adjusted to fit the experimentally found electron energy dependence [31]. Since there is no experimental data for deuterium, we multiplied the deuterium cross sections by the same fitting factors (adjusting the theoretical data to experiment) as used for hydrogen.

A large number of cross sections have been calculated recently for hydrogen [27] and deuterium [32]. We adopted their data for the processes of vibrational excitation by high-energy electrons (E-V), dissociation (DS), and molecular ionization (IZ-m). The meaning of the labels and the indicated reactions are explained in Table I. Other cross sections calculated using more elaborate theoretical methods are available for hydrogen, some of which are not in quantitative agreement with those of Ref. [27]. For the important E-V cross section, it should be noted that the results of Ref. [27] were shown therein to lie within the experimental error bar of the existing experimental data, at the lower limit. We chose the set of cross sections given in Refs. [27] and [32] for this study of the isotope effect, since their data were produced by the

same method for both hydrogen and deuterium.

The numerical simulations were carried out for the negative-ion source model studied in Ref. [9] (17 liter volume, surface area of 5100 cm²) at a filling pressure $P_f=3$ mTorr and discharge voltage of 100 V. We simulated hydrogen and deuterium sources, identical except for the working gas, with discharge currents in the range $I_d=10$ –500 A. The computer model calculates simultaneously the electron-energy distribution function (EEDF), the vibrational distribution, the dissociation fraction, and the densities of the positive- and negative-ion species in a zero-dimensional treatment of a bucket multipole ion source. The calculations are directly applicable to a single chamber multicusp source and the discharge region of a tandem source.

III. ISOTOPE EFFECT ON PLASMA PARAMETERS: THEORY AND EXPERIMENT

The isotope effect on plasma parameters predicted by the calculation agree very well with the measurements of Mullan and Graham in the discharge region of a tandem source [13]. In this section we will make a systematic comparison between our calculations and these measurements. The device studied experimentally was smaller than the model treated in the calculations—in terms of power density, the range of experimental studies correspond to the discharge current range of 2–40 A in our calculations.

As indicated in Fig. 1, calculations predict almost no isotope effect on the electron temperature T_e , in agreement with experiment. The calculated T_e is that temperature which well characterizes the low-energy part of the calculated EEDF, which also has a nonthermal tail at higher energy. Variation of the calculated plasma density n_e with I_d is shown in Fig. 2. We find that n_e is consistently higher in deuterium than in hydrogen. The ratio between n_e for the two gases is shown in Fig. 3, where it is seen that the ratio approaches but does not precisely

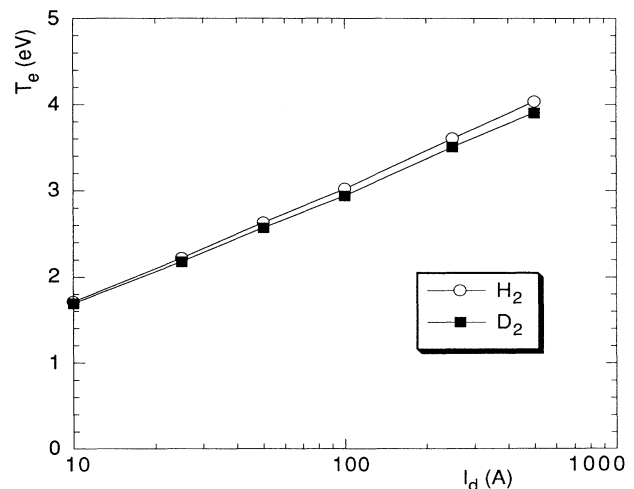


FIG. 1. Temperature of the thermal bulk of the EEDF as a function of the discharge current I_d , from the numerical model.

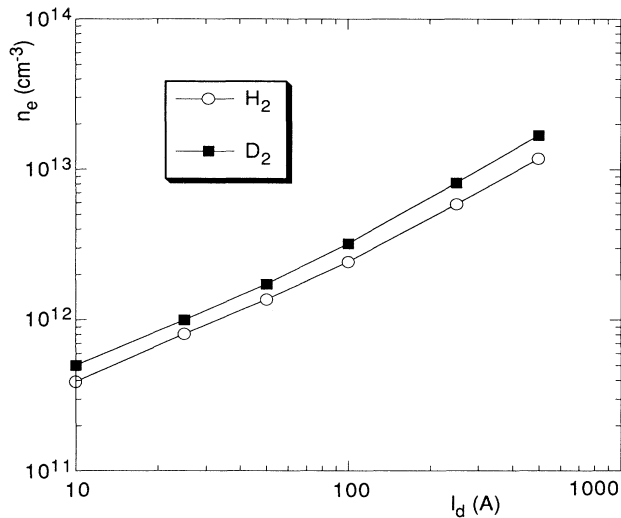


FIG. 2. Plasma density as a function of the discharge current I_d from the numerical model.

equal the $\sqrt{2}$ ratio which would result from different thermal speed at equal ion temperature. The calculations are consistent with the measurements of Mullan and Graham, which found the ratio of $n_e(\text{D}_2)$ to $n_e(\text{H}_2)$ approximately constant throughout the discharge and under various operating conditions, with an average value 1.20 ± 0.08 . This range, corresponding to their measurements, and the simple $\sqrt{2}$ prediction are indicated along with our data in Fig. 3.

Although we find practically no isotope effect on T_e , there is an isotope effect on the plasma potential V_p . The calculations find V_p consistently higher in deuterium discharges, as shown in Fig. 4. Repeating the analysis

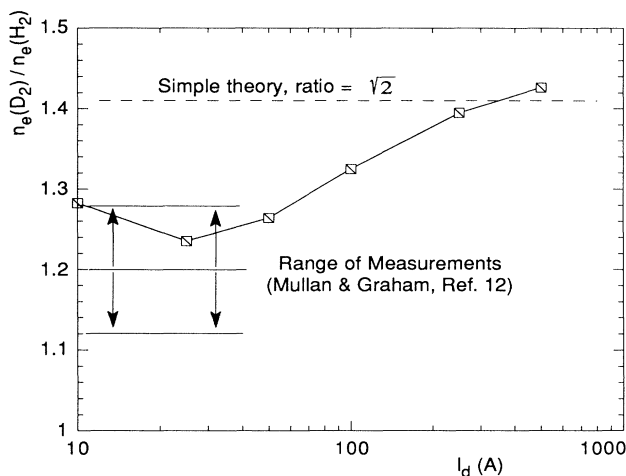


FIG. 3. Ratio of deuterium plasma density to hydrogen plasma density as a function of the discharge current I_d , from the numerical model. Dashed line indicates the simple thermal speed model (see text) and the limits between the arrows indicate the reported range of measurements in low power density discharges [13].

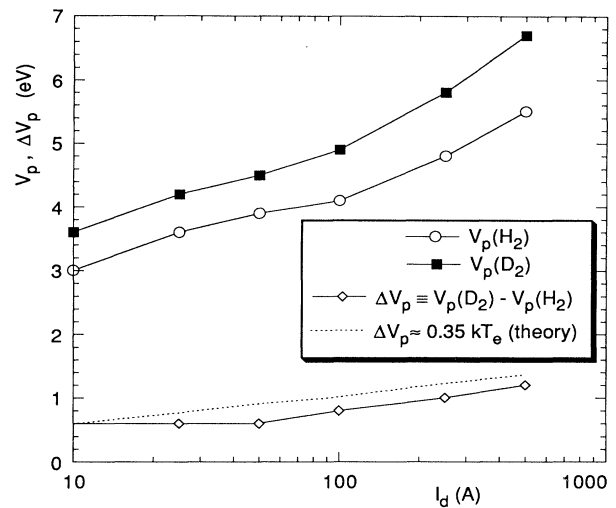


FIG. 4. Plasma potential in hydrogen and deuterium discharges as a function of the discharge current I_d , from the numerical model. Following the analysis of Ref. [13], ΔV_p is also plotted and compared with simple theory [33] for no magnetic confinement.

performed by Mullan and Graham for their experimental data, we plot $\Delta V_p = V_p(\text{D}_2) - V_p(\text{H}_2)$ for our calculated results along with a simple theoretical model [33] $\Delta V_p = \ln \sqrt{2} k T_e \approx 0.35 k T_e$ developed for a Maxwellian EEDF and no confining magnetic field. Our calculation agrees fairly well with this simple theory, as did the measurements of Mullan and Graham, despite the fact that the theory is not strictly applicable to a multicusp-confined plasma.

Figure 5 indicates the fraction of dissociated gas predicted by the calculation for both working gases. With our assumptions that $T_D = T_H$ and $\gamma_D = \gamma_H$, the wall recombination rate is slower for the slower D atoms, and

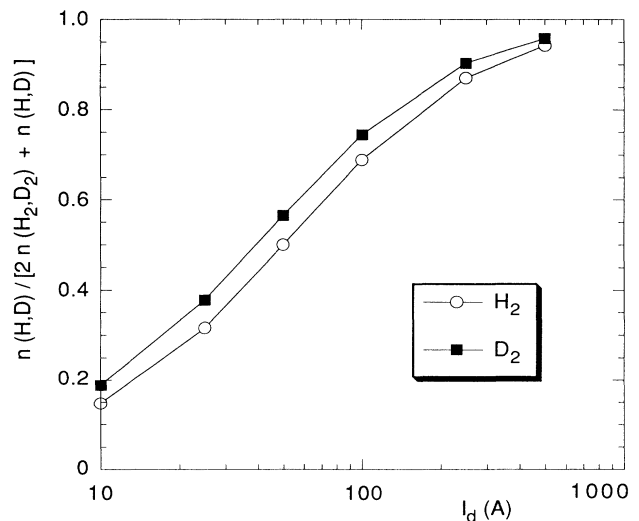


FIG. 5. Fraction of dissociated gas, predicted by the numerical model, as a function of the discharge current I_d .

deuterium is more dissociated than hydrogen. This is perhaps the most significant isotope effect, due to the poisonous effect of atoms on the vibrational distribution, which will be discussed in Sec. IV. Taking a value γ_D smaller than γ_H , as discussed in Sec. II, would intensify this isotope effect.

The degree of gas dissociation affects the ion fraction—since there is more D than H, then D^+ ions constitute a larger fraction of the total ion density than do H^+ ions at the same discharge current. (Such a difference has been observed in the extraction region [14].) In the model, H^+ and D^+ ions are more energetic than the other positive ions and thus leave the system more rapidly. This effect explains, at least in part, the departure of the $n_e(D_2)/n_e(H_2)$ ratio from the simple $\sqrt{2}$ theory (Fig. 3). Note that in the highest power calculations where both hydrogen and deuterium are highly dissociated, H^+ or D^+ ions form the bulk of the positive-ion population, and $n_e(D_2)/n_e(H_2) \approx \sqrt{2}$.

IV. THE VIBRATIONAL DISTRIBUTION AND NEGATIVE-ION PRODUCTION

Vibrational spectra $H_2(v'')$ and $D_2(v'')$ were calculated by the simulation code over the range of conditions studied, $P_f = 3$ mTorr and $I_d = 10$ –500 A. Examples of these calculated spectra for a 50-A discharge are shown in Fig. 6. In this plot the density of each vibrational state $H_2(v'')$ or $D_2(v'')$ is normalized by its width $\Delta\epsilon_{vib}(v'') = [\epsilon_{vib}(v''+1) - \epsilon_{vib}(v''-1)]/2$ (i.e., $\Delta\epsilon_{vib}$ reflects the spacing of vibrational levels on the vibrational energy axis). This presentation, showing the vibrational state density per unit vibrational energy, is more useful for exhibiting the isotope effect than a direct comparison

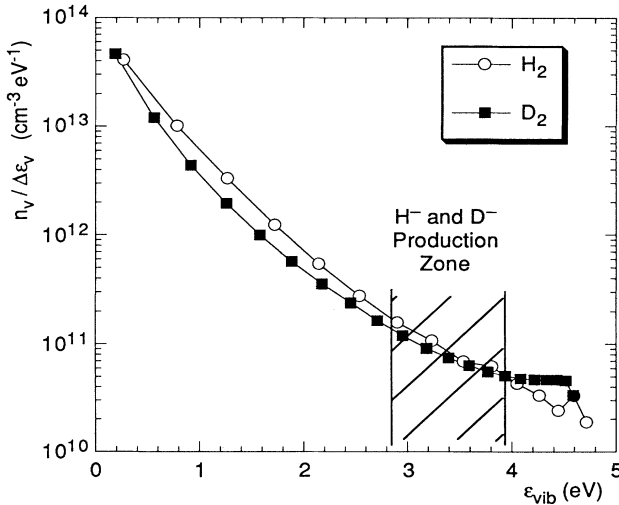


FIG. 6. Vibrational spectra, with vibrational populations normalized to spacing between vibrational levels (see text), predicted by the model for the $P_f = 3$ mTorr, $I_d = 50$ A case. Hatched area indicates vibrational levels principally responsible for negative-ion creation via DA.

of spectra, because deuterium has more vibrational states among which the vibrationally excited molecules are distributed. Our calculations show that negative-ion production from $H_2(\epsilon_{vib})$ and $D_2(\epsilon_{vib})$ mainly involves several high-lying states indicated by the hatched area in Fig. 6. In this example, the $H_2(\epsilon_{vib})$ and $D_2(\epsilon_{vib})$ spectra are nearly identical in the negative-ion production region $\epsilon_{vib} \approx 3.4 \pm 0.5$ eV. The DA cross sections for negative-ion production are similar functions of ϵ_{vib} for H and D. Thus there would be little isotope effect on negative-ion production by DA for the illustrated vibrational spectra and a given electron distribution.

Negative ions are produced by dissociative attachment of electrons from the thermal bulk of the EEDF with $H_2(v'')$ or $D_2(v'')$. The region most important for negative-ion production may be characterized by a different T_e and/or n_e than the excitation region where molecules are vibrationally excited by energetic electrons. Such a spatial separation may be important in the operation of the tandem source (with two regions separated by a magnetic filter) and the hybrid source (with the energetic electrons confined in the multicusp fields). We use the vibrational spectra calculated for the discharge region to calculate dissociative attachment in some nearby negative-ion production region. This approach is based on the approximation that each region is uniform and it neglects vibrational cooling during transport between the two regions and across the production region [34].

To proceed in a general way, consider H^- and D^- production in the production region from (a) the calculated spectra f_{vib} , which vary with I_d and P_f , and (b) the local electron distribution f_e , which is assumed to be a Maxwellian distribution specified by n_e and T_e . The negative-ion production rate P_- thus depends on I_d and P_f via the vibrational spectrum $f_{vib}(I_d, P_f)$ predicted by the discharge region simulation, and on n_e and T_e , which characterize the second region where negative ions are produced.

The negative-ion production rate per unit volume $P_-(n_e, T_e; f_{vib}(I_d, P_f))$ depends linearly on n_e , so we will consider the negative-ion production ratio $\Pi_-(T_e; f_{vib}(I_d, P_f)) \equiv P_-/n_e$,

$$\Pi_- = \frac{\sum_{v''} \langle n(v'') \sigma_{DA}(v'') v_e \rangle}{\sum_{v''} n(v'') \int_0^\infty \sigma_{DA}(\epsilon; v'') v_e(\epsilon) f_e(\epsilon) d\epsilon} = \frac{\int_0^\infty f_e(\epsilon) d\epsilon}{\int_0^\infty f_e(\epsilon) d\epsilon}, \quad (2)$$

where the EEDF $f_e(\epsilon; n_e, T_e)$ is a Maxwellian distribution and $n(v''; I_d, P_f)$ are vibrational densities. We will study how $\Pi_-(T_e; I_d, P_f)$ varies with T_e and the discharge conditions.

The production ratio $\Pi_-(T_e; I_d, P_f)$ is plotted in Fig. 7 for hydrogen and deuterium discharges with $I_d = 10, 50, 100,$ and 250 A and $P_f = 3$ mTorr. The temperature dependence is quite similar for hydrogen and deuterium over a large range of I_d , with Π_- rising rapidly as T_e approaches the optimal temperature of $T_e^{opt} \approx 0.6$ – 0.8 eV and then falling more slowly as T_e increases beyond T_e^{opt} . $\Pi_-(T_e)$ is somewhat more peaked about T_e^{opt} in deuteri-

um discharges than in hydrogen. Varying the discharge conditions by varying I_d essentially rescales $\Pi_-(T_e)$, which maintains its characteristic dependence on T_e . We express this explicitly by defining

$$\bar{\Pi}_-(T_e) = \Pi_-(T_e; I_d, P_f) / \Pi_-^{\text{opt}}(I_d, P_f)$$

$$\text{with } \Pi_-^{\text{opt}}(I_d, P_f) \equiv \Pi_-(T_e = T_e^{\text{opt}}; I_d, P_f) \quad (3)$$

so that the characteristic dependence $\bar{\Pi}_-(T_e)$ is normalized to unity at $T_e = T_e^{\text{opt}}$. Figure 8 plots the average value of $\bar{\Pi}_-(T_e)$ as a solid line, where the average is taken over the ensemble of calculations with $I_d = 10, 25, 50, 100,$ and 250 A in both hydrogen and deuterium. The dotted lines plot the minimum and maximum values of $\bar{\Pi}_-(T_e)$ over the same ensemble, indicating the limited variation of $\bar{\Pi}_-(T_e)$ for the two isotopes and a large

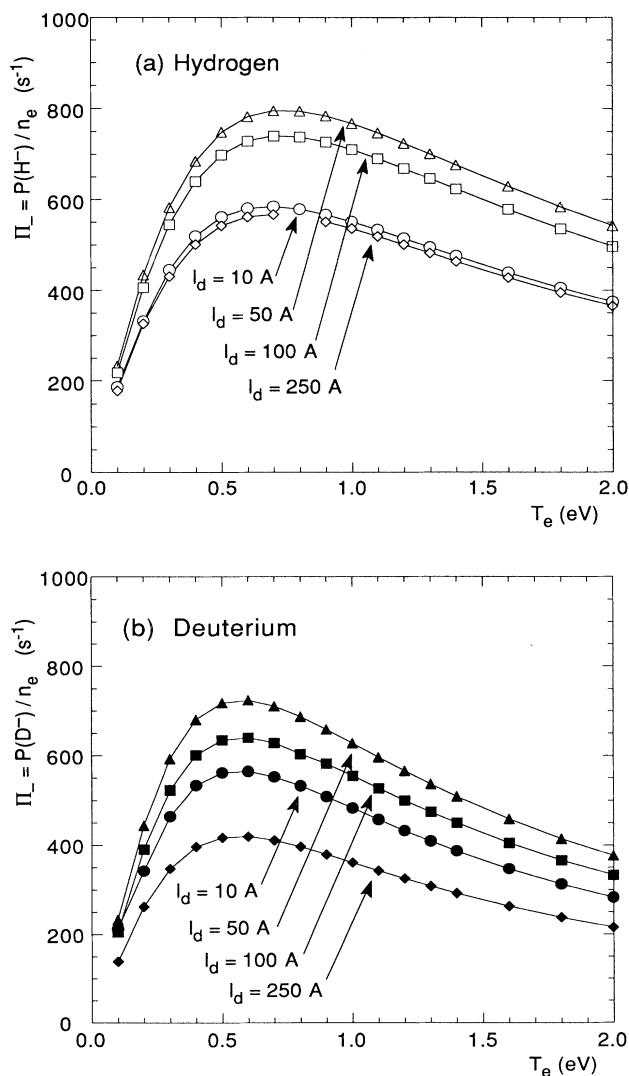


FIG. 7. Production ratio Π_- of negative ions [see text and Eq. (2)] from the calculated vibrational spectra and an arbitrary Maxwellian EEDF as a function of T_e , for (a) hydrogen discharge and (b) deuterium discharge.

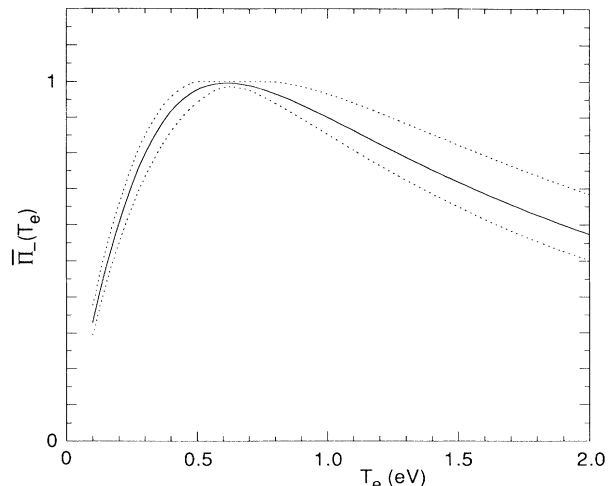


FIG. 8. —, plots average of $\bar{\Pi}_-$ over the ensemble of calculations (hydrogen and deuterium discharges with $I_d = 10, 50, 100,$ and 250 A and $P_f = 3$ mTorr), while $\cdot \cdot \cdot$ indicates the maximum and minimum values of $\bar{\Pi}_-$ over the same ensemble.

change in discharge current.

The shape of $\bar{\Pi}_-(T_e)$ is determined by the dissociative attachment rate of coefficients $\langle \sigma v \rangle_{\text{DA}}$. Figure 9 shows the T_e dependence of $\langle \sigma v \rangle_{\text{DA}}$ for all vibrational levels v'' of hydrogen, based on the $J = 1$ cross sections calculated using a program furnished by Wadehra [30]. These rate coefficients for different vibrational levels v'' vary by orders of magnitude. To show the T_e dependence on a single figure, $\langle \sigma v \rangle_{\text{DA}}(T_e)$ for each $v'' \leq 9$ is normalized to 1 at its peak value. For the exothermic reactions from

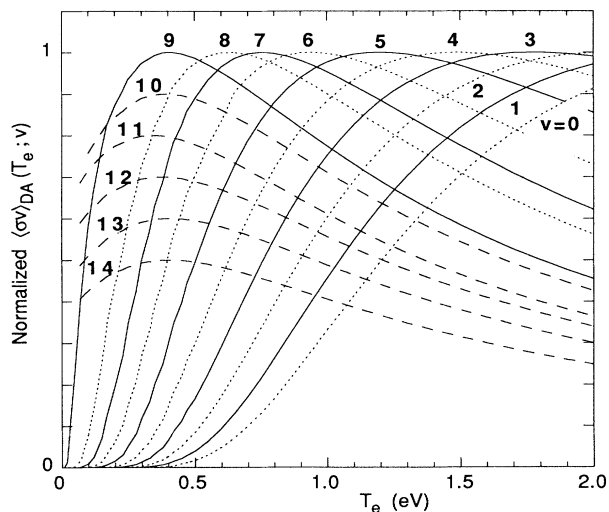


FIG. 9. — and $\cdot \cdot \cdot$ show the T_e dependence of the dissociative attachment rate coefficients $\langle \sigma v \rangle_{\text{DA}}$ for hydrogen used in the numerical model, normalized to unity for $v'' \leq 9$. The $v'' \geq 10$ rate coefficients for exothermic attachment, indicated by $- - -$, have a similar T_e dependence and are normalized to $0.9, 0.8, \dots, 0.5$ to distinguish them on the plot.

$v'' \geq 10$, $\langle \sigma v \rangle_{\text{DA}}(T_e)$ are very similar when normalized to 1—to distinguish them on the plot, these rate coefficients are normalized to various values < 1 . The $v'' = 6-8$ curves in Fig. 9 peak at temperatures corresponding to the maximum in Fig. 8. The actual peak value attained along each $\langle \sigma v \rangle_{\text{DA}}(T_e)$ curve is designated by the solid diamond in Fig. 10, where it is plotted against v on both linear and logarithmic scales. A better indication of the importance of the different vibrational levels to negative-ion production is indicated by the second curve, indicated by the open triangle, which shows the effect of weighting the peak $\langle \sigma v \rangle_{\text{DA}}$ values by the vibrational densities of a “typical” spectrum [in this case, the calculated $H_2(v'')$ spectrum shown in Fig. 6]. The weighted values are arbitrarily rescaled for display on the same plot, on both linear and logarithmic scales. With this weighting, the $v'' = 6-9$ levels are seen to be most important.

The T_e dependence of negative-ion production may be shown explicitly, as

$$P_- \approx n_e \Pi_-^{\text{opt}}(I_d, P_f) \bar{\Pi}_-(T_e), \quad (4)$$

where for $\bar{\Pi}_-(T_e)$ we adopt the average value plotted as a solid line in Fig. 8. Equation (4) may be rewritten in a slightly different form which is useful in scaling arguments,

$$P_- \approx c_{\sigma^*} n_e n_{v^*} \bar{\Pi}_-(T_e), \quad (5)$$

where n_{v^*} represents the density of the vibrational levels most important for negative-ion production and c_{σ^*} is a constant which depends on the DA rate coefficients of these vibrational levels. The quantity n_{v^*} may be defined in several ways [e.g., simply as the population of $H_2(v'' = 7)$ or $D_2(v'' = 10)$, or in a more sophisticated way

as a weighted average over the states most important for DA]. Once a specific definition of n_{v^*} is adopted, then c_{σ^*} follows from $\Pi_-^{\text{opt}} = c_{\sigma^*} n_{v^*}$. A good definition of n_{v^*} will permit $\Pi_-^{\text{opt}} \approx c_{\sigma^*} n_{v^*}$ to be satisfied over a range of operating conditions with a single constant c_{σ^*} . For the purpose of discussing scaling laws, we assume such a “good” definition of n_{v^*} and c_{σ^*} without entering into details. We see that Π_-^{opt} and n_{v^*} both indicate the level of vibrational excitation. In a negative-ion source, the three quantities n_e , n_{v^*} , and T_e vary with discharge conditions. If the ideal temperature $T_e = T_e^{\text{opt}}$ could be maintained, then $P_-^{\text{opt}}/n_e \equiv \Pi_-^{\text{opt}} \approx c_{\sigma^*} n_{v^*}$ and the production ratio would depend only on the vibrational distribution.

The I_d variation of the calculated production ratio Π_-^{opt} is shown in Fig. 11. At $I_d = 10$ A, Π_-^{opt} is nearly the same for D^- and H^- production. Π_-^{opt} reaches a maximum at $I_d = 30-40$ A in both deuterium and hydrogen. Π_-^{opt} shows little variation between the calculations at $I_d = 25$ and 50 A. As I_d further increases, Π_-^{opt} decreases more rapidly for deuterium than for hydrogen. It is 15% lower for D^- production than for H^- production by $I_d = 50$ A, and 40% lower at $I_d = 500$ A.

The calculation indicates that an isotope effect at high discharge current reduces the D^- production by comparison with H^- production. The higher degree of dissociation in deuterium is largely responsible for this reduction, causing increased V-t cooling of the vibrational distribution by atoms. We have assumed $T_D = T_H$ and $\gamma_D = \gamma_H$ in this modeling exercise. If in fact $\gamma_D < \gamma_H$, as was discussed in Sec. II, this isotope effect would be stronger.

To proceed from negative-ion production to negative-ion density,

$$n_- \approx \frac{c_{\sigma^*} n_e n_{v^*} \bar{\Pi}_-(T_e)}{n_e \langle \sigma v \rangle_{\text{MN}} + n_{\text{at}} \langle \sigma v \rangle_{\text{AD}} + \tau_{\text{wx}}^{-1}}, \quad (6)$$

would require knowledge of loss processes. Too little is known to establish the isotope dependence of negative-ion destruction. Three potentially important loss pro-

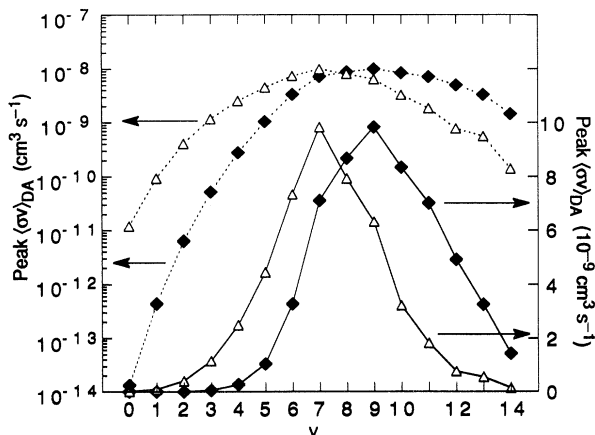


FIG. 10. At each vibrational level v'' of hydrogen, \blacklozenge indicates the maximum value attained by $\langle \sigma v \rangle_{\text{DA}}$ as T_e is varied, on both logarithmic ($\cdots \blacklozenge \cdots$) and linear ($\text{---} \blacklozenge \text{---}$) scales. The effect of weighting these peak values by the vibrational populations of a “typical” spectrum $H_2(v'')$ (that of Fig. 6, see text) is indicated by \triangle . The weighted values are arbitrarily renormalized for convenient display and plotted on both logarithmic ($\cdots \triangle \cdots$) and linear ($\text{---} \triangle \text{---}$) scales.

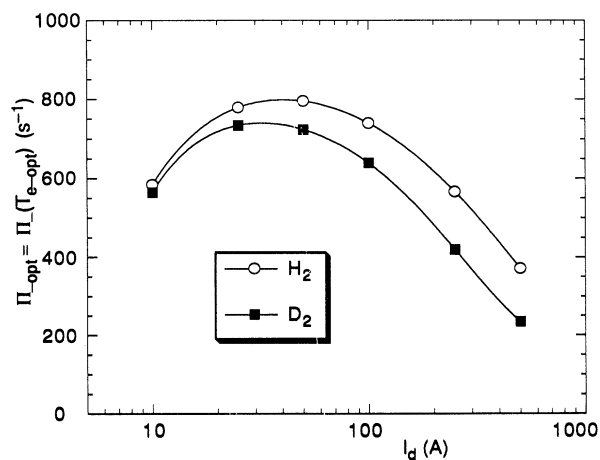


FIG. 11. The optimum production ratio $\Pi_-(T_e = T_{e-\text{opt}})$ predicted by the numerical model for hydrogen and deuterium.

cesses are indicated in the denominator of Eq. (6): mutual neutralization, $H^- + \{H_2^+, H_3^+\} \rightarrow H + \dots$; associative detachment, $H^- + H \rightarrow e + H_2$; and wall loss and extraction loss characterized by the τ_{wx} loss time. There is at least a factor of 2 uncertainty in the $\langle\sigma v\rangle_{MN}$ and $\langle\sigma v\rangle_{AD}$ rate coefficients, so it is not clear which of these volume destruction processes is dominant. Wall loss may be significant in some cases—the sheath potential must be reduced enough to permit negative-ion extraction, which may occasion losses on the walls of the extraction region as well as through the extraction orifice(s).

The isotope effect on MN losses may be estimated using Hickman's [35] scaling law $\langle\sigma v\rangle_{MN} \propto (\mu T)^{-1/2}$ for reduced mass μ and temperature T . Measurements effected in a hybrid source found the H^- temperature to be approximately twice the D^- temperature over a range of operating conditions [17]. The colder D^- temperature nearly cancels the decrease in $\langle\sigma v\rangle_{MN}$ due to the increased mass of deuterium, giving similar loss rates in hydrogen and deuterium. For AD, there is no direct information about isotope effects. We note that for $H+H^-$ the theoretically predicted $\langle\sigma v\rangle_{AD}$ is quite insensitive to H and H^- energy for particle energies below 1 eV [36]. To the extent that isotope dependence of $\langle\sigma v\rangle_{AD}$ enters through particle velocities, there would be no isotope effect. The larger mass and reduced temperature together would halve wall losses for D^- . This discussion suggests that the D^- loss rate may be comparable to that of H^- if volume loss processes dominate, but halved if wall loss dominates.

V. NEGATIVE-ION MEASUREMENTS IN THE HYBRID SOURCE

Some experimental results are presented here for H^- and D^- ions produced in a hybrid multicusp ion source. The source [37,38] is a cylindrical stainless-steel chamber surrounded by ten samarium-cobalt magnets. The primary electrons are produced by ten thoriated tungsten filaments biased 50-V negative with respect to the chamber walls. These filaments are located in the multicusp magnetic field, so the primary electrons are trapped and confined in the neighborhood of the cylindrical sidewall. There are few energetic electrons in the magnetic-field-free central region, and the electron temperature is low there; this is a favorable condition for H^- or D^- production. It is interesting to compare the predictions of Sec. IV with measurements in this large uniform production region, even though the simulation code described earlier is not well adapted to the hybrid excitation region. The negative-ion density has been studied using photodetachment associated with optogalvanic detection by an electrostatic probe [39].

The isotope effect on plasma parameters in a hybrid source is different from that in a tandem source. There is a negligible isotope effect on the plasma density, as evident in Fig. 12 and the ensemble of experimental data, but there is an effect on the electron temperature [18]. This is the opposite of the situation discussed in Sec. III for both calculations and measurements in a tandem discharge region. The numerical simulation code does

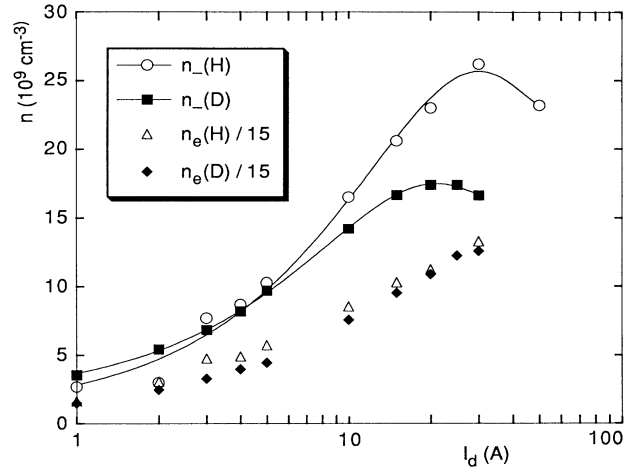


FIG. 12. Negative-ion density n_- and scaled-down electron density n_e measured in the hybrid source as a function of the discharge current I_d , at $P_f = 3$ mTorr.

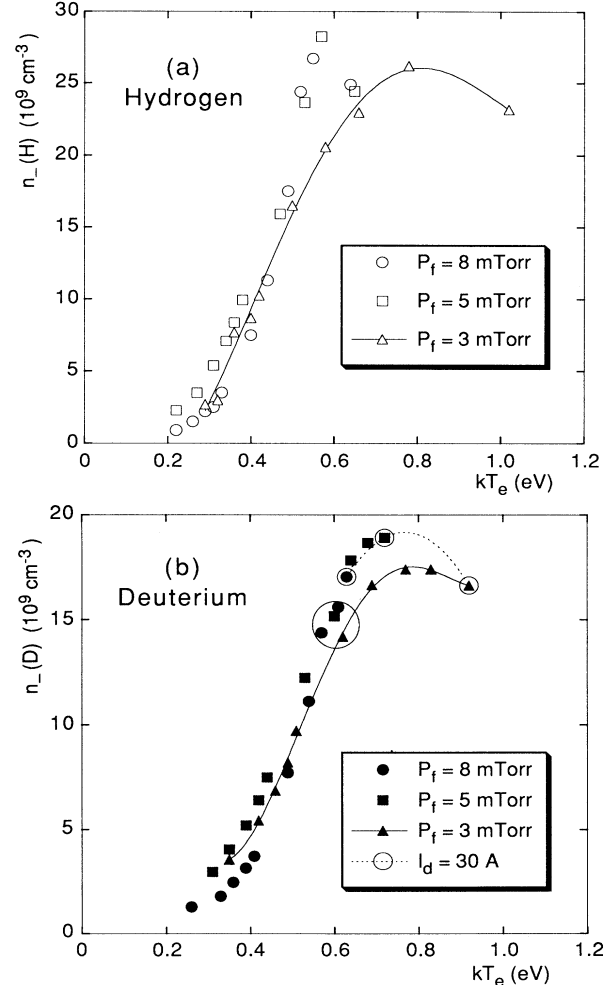


FIG. 13. Measured negative-ion density n_- , for several values of filling pressure P_f , as a function of the measured electron temperature T_e . All measurements made at the center of the hybrid source in (a) a hydrogen discharge and (b) a deuterium discharge. The four data points enclosed by the large circle in (b) are discussed in the text.

not model the geometry of the hybrid source, which must be responsible for its distinctive behavior.

Figure 12 plots data taken at $P_f = 3$ mTorr against I_d . It shows that D^- and H^- densities are comparable for low power discharges. However, at higher values of the discharge current, the measured negative-ion density is lower in deuterium than in hydrogen discharges. The peak D^- density is approximately 66% of the peak H^- density.

Figure 13 shows the H^- and D^- densities measured [17,18] by a photodetachment technique in the center of the hybrid multicusp ion source, plotted as a function of the measured electron temperature T_e . The measurements were made at three values of the filling pressure, $P_f = 3, 5,$ and 8 mTorr, while varying the discharge current from 1 to 50 A. For both hydrogen and deuterium, the negative-ion density at constant P_f lies along a characteristic curve with a maximum at $T_e^{\text{opt}} \approx 0.6\text{--}0.8$ eV. In Fig. 13(b), the three points connected by a dotted line for $I_d = 30$ A are seen to fit a similarly shaped curve. At a given electron temperature, H^- or D^- shows only a weak variation for a large variation in P_f , I_d , and n_- . The four data points enclosed by a circle in Fig. 13(b) illustrate this variation, for they cover the range $P_f = 3\text{--}8$ mTorr, $I_d = 10\text{--}25$ A, and $n_- = (1.1\text{--}3.2) \times 10^{11}$ cm^{-3} while T_e and n_- vary only 10%. T_e is obviously an important parameter in determining negative-ion density.

It is very interesting to compare the characteristic form of the measured negative-ion density, from Fig. 13, with the calculated production ratio $\bar{\Pi}_-(T_e)$ of Fig. 8. There are maxima which occur at similar values of T_e . One would not expect the curves to be identical, since the negative-ion density depends not only on the normalized production rate $\bar{\Pi}_-(T_e)$ but also on the molecular vibrational spectrum and the negative-ion destruction rate.

VI. NEGATIVE-ION DENSITY MEASUREMENTS IN A TANDEM SOURCE

The negative-ion density in the small tandem source described in Sec. III has been recently measured for both hydrogen and deuterium discharges [19]. In a tandem source, it is not immediately obvious whether most negative ions in the extraction region are originally produced in the discharge region or are locally produced in the extraction region. These measurements found a higher negative-ion density in the extraction region than in the discharge region, suggesting local production. We identify the production region of our theory with the extraction region of the tandem. We will thus consider the measurements of the H^- and D^- densities reported for the extraction region.

Negative-ion density measurements were reported for $I_d = 10\text{--}100$ A at $P_f = 2$ mTorr. H^- density increased approximately linearly with discharge current up to $I_d = 40$ A, then saturated with almost no further increase between $I_d = 80$ and 100 A. D^- density showed the same variation with I_d , being approximately 75% of the H^- density at each value of I_d .

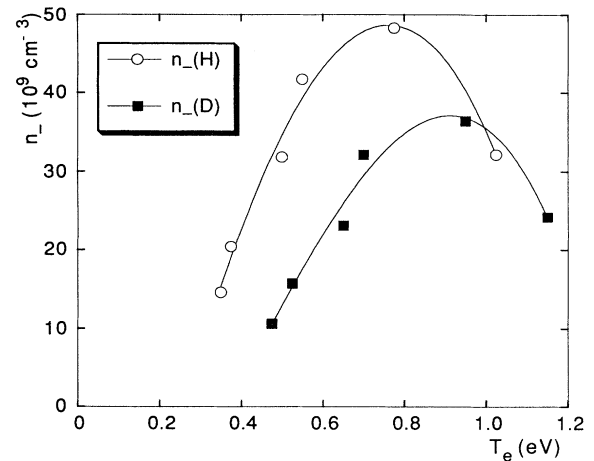


FIG. 14. Negative-ion density n_- plotted against electron temperature T_e , both measured in the extraction region of a tandem source.

We have examined the T_e dependence of negative-ion density by combining the new photodetachment data [19] with previously published measurements of plasma parameters in the extraction region [14]. The result is shown in Fig. 14, for fixed $I_d = 10$ A and $P_f = 1\text{--}10$ mTorr. The H^- and D^- densities have maxima at $T_e \approx 0.8$ and 0.9 eV, respectively, and the T_e dependence is similar to the hybrid results of Fig. 13 and to the calculated production ratio $\bar{\Pi}_-(T_e)$ of Fig. 8.

VII. DISCUSSION

In Sec. IV we discussed the negative-ion loss mechanisms, which tend to be equal or weaker in deuterium than in hydrogen. We advanced an argument for minimal isotope effect on negative-ion destruction if volume losses dominate losses to the walls—but too little is known about the loss mechanisms to support an authoritative assertion to this effect. Thus we limit our comparison of negative-ion density measurements with negative-ion production calculations to two general observations: (a) the general variation as discharge current I_d is increased; and (b) the variation around the optimum temperature $T_e^{\text{opt}} \approx 0.6\text{--}0.8$ eV predicted by calculations.

The vibrational excitation is characterized by $P_-^{\text{opt}}/n_e \equiv \Pi_-^{\text{opt}} \approx c_{\sigma^*} n_{v^*}$, shown in Fig. 11. The I_d dependence of the H^- and D^- densities measured in the hybrid source is qualitatively consistent with the calculation, as seen by comparing Fig. 12 with the calculated I_d variation of Π_-^{opt} of Fig. 11. There is almost no isotope effect at low discharge current, but an increasing disparity between H^- and D^- densities as I_d is increased. In the tandem extraction region, the measured H^- and D^- densities at first increased linearly with I_d , then saturated as I_d further increased. The measured D^- density was lower than the H^- density at all values of discharge current.

At saturation, the measured D^- density is approximately 34% lower than the H^- density in the hybrid

source and 25% in the tandem source. Saturation occurred at $I_d = 20\text{--}30$ A in the hybrid and $I_d = 80\text{--}100$ A in the tandem. By comparison, the calculated Π^{opt} saturates at $I_d = 30\text{--}40$ A, where the isotopic difference is smaller than measured for negative-ion density. Note that when $\Pi^{\text{opt}}(I_d)$ is plotted on a linear scale (rather than on the logarithmic scale of Fig. 11), $\Pi^{\text{opt}}(I_d)$ is roughly constant over a broad region $25 \text{ A} < I_d < 75 \text{ A}$. A direct comparison between theory and experiment is not possible, since the negative-ion density depends on destruction processes as well. In our model we assumed no isotope effect on atomic temperature and wall recombination probability γ , because of the paucity of available experimental evidence. Measurements are needed to establish the actual isotope effect on atomic density. We noted that an increased D^+ fraction measured in the tandem source is consistent with the predicted higher dissociation in deuterium.

A local maximum in measured negative-ion density $n_-(T_e)$ was demonstrated for constant P_f (varying I_d) in the hybrid and for constant I_d (varying P_f) in the tandem and in the hybrid. We recall that similar behavior was observed in a magnetic-field-free diffusion-type plasma [40], but for the ratio n_-/n_e rather than n_- . It would be interesting to examine both n_- and n_-/n_e in the tandem extraction region for constant P_f (varying I_d), but the published data do not permit such a comparison.

Simple scaling laws may be derived to indicate that either n_- or n_-/n_e should be proportional to $\bar{\Pi}_-(T_e)$, depending on the assumptions taken. We sketch two plausible examples for scaling with I_d . These two examples follow from a number of assumptions: Assume that MN is the dominant negative-ion loss process, so that Eqs. (5) and (6) yield $n_- \propto n_{v*} \bar{\Pi}_-(T_e)$. Assume that n_{v*} is determined by the balance between E-V excitation and cooling by either wall or atomic V-t collisions. As I_d increases, the energetic electron density increases, so assume that ionization, dissociation, and E-V excitation increase linearly with I_d . The two scaling laws now follow from different assumption about vibrational cooling: (1) When vibrational cooling is dominated by atomic V-t collisions, then n_{v*} production and destruction terms both increase with I_d (since atomic density $\propto I_d$), so that n_{v*} is saturated and $n_- \propto \bar{\Pi}_-(T_e)$. (2) When wall collisions dominate vibrational cooling, $n_{v*} \propto I_d$. If positive ions are predominantly lost to the walls rather than by dissociative recombination, then $n_e \propto I_d$ and we obtain the alternative scaling $n_-/n_e \propto n_-/n_{v*} \propto \bar{\Pi}_-(T_e)$. This second scaling law is equivalent to that derived in Refs. [40] and [41].

VIII. CONCLUSIONS

We have used a numerical model to study the isotope effect on plasma parameters and negative-ion production in hydrogen and deuterium multicusp discharges. For the isotope effect on plasma parameters (n_e, T_e, V_p), there is good qualitative agreement between predictions of the

model and measurements performed in the discharge region of a tandem source. The model treats the complicated problem of plasma confinement by multipole magnetic fields in a quite simplistic manner by using equivalent loss surfaces—the good agreement on plasma parameters shows the usefulness of this approach.

Negative-ion production was studied with a two step method: the numerical model was used to calculate vibrational distributions for $\text{H}_2(v'')$ and $\text{D}_2(v'')$ in a discharge region, then negative-ion production from these distributions was found as a function of local n_e and T_e in an adjoining production region. Since the isotope effect on vibrational cooling in wall collisions is unknown, we chose condition which favored atomic V-t vibrational cooling by studying a large volume source and by avoiding low-power cases.

The calculation indicates little isotope difference in vibrational excitation at the lower discharge currents examined. The discussion following Eq. (5) showed how the vibrational excitation is indicated by Π^{opt} , which is shown in Fig. 11 where it is seen to attain a maximum at $I_d = 30\text{--}40$ A. Because of the higher atomic density in deuterium discharges, the vibrational cooling from atomic V-t collisions is more important in deuterium than in hydrogen. This causes the most significant isotope effect seen in the simulations: decreased vibrational excitation in deuterium discharges compared to hydrogen discharges at high power.

We discussed the I_d dependence of the negative-ion density measured in the tandem source extraction region and the hybrid source center. In both sources, the negative-ion density saturated with increasing discharge current I_d . D^- density was lower than H^- density at saturation in both sources. In the hybrid source, D^- density increasingly diverged from H^- density as I_d was increased. This is qualitatively consistent with the calculated variation of vibrational excitation. In the tandem source, however, the ratio of the measured H^- and D^- densities was approximately constant as I_d was increased.

In Eqs. (2)–(5) we sketched how the role of T_e in negative-ion production may be separated from role of n_e and the level of vibrational excitation. The calculations predict an optimal electron temperature $T_e^{\text{opt}} \approx 0.6\text{--}0.8$ eV for negative-ion production in both hydrogen and deuterium discharges. This was true over a wide variation in discharge current. The T_e dependence is summarized by $\bar{\Pi}_-(T_e)$ and shown in Fig. 8. We showed how this characteristic form is related to the T_e dependence of the dissociative attachment rate coefficients used in the calculation, illustrated in Fig. 10. This result of the calculation is more general than the specific geometry and operating conditions considered here.

We demonstrated a maximum of negative-ion density $n_-(T_e)$ at $T_e^{\text{opt}} \approx 0.8\text{--}0.9$ eV by analyzing photodetachment measurements in the central field-free region of a hybrid source and in the extraction region of a tandem source, for both hydrogen and deuterium discharges. It must be admitted that this demonstration rests on relatively few data points with $T_e > T_e^{\text{opt}}$. The recurrence of the local maximum in both experiment and theory at

similar values of T_e^{opt} lends support to the theoretical picture which has been constructed to explain negative volume ion production through dissociative attachment. For this tandem source, the agreement supports the conclusion that negative ions in the extraction zone are locally produced—the negative-ion density maximum occurs when T_e in the extraction region, rather than T_e in the discharge region, is near T_e^{opt} .

ACKNOWLEDGMENTS

The authors would like to express their appreciation to M. Capitelli, C. Gorse, A. Laganà, and J. M. Wadehra for providing us with rate constant and cross-section data for the simulation, and to A. Al-Jibouri and W. G. Graham for early access to their negative-ion density measurements.

*Electronic address: skinner@lpmi.polytechnique.fr

- [1] G. W. Hamilton and M. Bacal, *IEEE Trans. Plasma Sci.* **19**, 1143 (1991).
- [2] A. J. T. Holmes, *Plasma Phys. Controlled Fusion* **34**, 653 (1992).
- [3] M. Bacal, *Nucl. Instrum. Methods Phys. Res. B* **37/38**, 28 (1989).
- [4] M. Bacal and D. A. Skinner, *Comments At. Mol. Phys.* **23**, 283 (1990).
- [5] J. N. Bardsley and J. M. Wadehra, *Phys. Rev. A* **20**, 1398 (1979).
- [6] P. Berlemont, D. A. Skinner, and M. Bacal, *Rev. Sci. Instrum.* (to be published).
- [7] G. C. Stutzin, Ph.D. thesis, University of California—Berkeley, 1991.
- [8] M. Capitelli, C. Gorse, P. Berlemont, D. A. Skinner, and M. Bacal, *Chem. Phys. Lett.* **179**, 48 (1991).
- [9] D. A. Skinner, P. Berlemont, and M. Bacal, in *Proceedings of the 5th International Symposium on the Production and Neutralization of Negative Ions and Beams, Brookhaven*, edited by Ady Herschcovitch, AIP Conf. Proc. No. 210 (AIP, New York, 1990), p. 557.
- [10] J. R. Hiskes and A. M. Karo, *Appl. Phys. Lett.* **54**, 508 (1989).
- [11] P. J. Eenshuistra, R. M. A. Heeren, A. W. Kleyn, and H. J. Hopman, *Phys. Rev. A* **40**, 3613 (1989).
- [12] T. Inoue, G. D. Ackerman, W. S. Cooper, M. Hanada, J. W. Kwan, Y. Ohara, Y. Okumura, and M. Seki, *Rev. Sci. Instrum.* **61**, 496 (1990).
- [13] A. A. Mullan and W. G. Graham, *Rev. Sci. Instrum.* **61**, 451 (1990).
- [14] A. A. Mullan and W. G. Graham, *J. Phys. D* **24**, 1533 (1991).
- [15] R. McAdams, R. F. King, and A. F. Newman, in *Proceedings of the 4th European Workshop on the Production and Application of Light Negative Ions*, edited by W. G. Graham (The Queen's University of Belfast, Belfast, 1991), p. 13.
- [16] A. J. T. Holmes, L. M. Lea, S. B. Wells, R. S. G. Parker, and M. Inman, AEA Industrial Technology, Culham Laboratory, AEA Fusion Report No. 185, Abingdon, UK 1992.
- [17] R. Leroy, M. Bacal, P. Berlemont, C. Courteille, and R. A. Stern, *Rev. Sci. Instrum.* **63**, 2686 (1992).
- [18] R. Leroy, Ph.D. thesis, Ecole Polytechnique Palaiseau, 1991.
- [19] A. Al-Jibouri and W. G. Graham, in *Proceedings of the 6th International Symposium on the Production and Neutralization of Negative Ions and Beams, Brookhaven*, 1992, edited by Ady Herschcovitch and James G. Alesi, AIP Conf. Proc. No. 287 (AIP, New York, in press).
- [20] P. Berlemont, D. A. Skinner, and M. Bacal, in *Proceedings of the 6th International Symposium on the Production and Neutralization of Negative Ions and Beams, Brookhaven*, 1992 (Ref. [19]).
- [21] D. A. Skinner and P. Berlemont, in *Proceedings of the 4th European Workshop on the Production and Application of Light Negative Ions* (Ref. [15]), p. 1.
- [22] C. Gorse, M. Capitelli, M. Bacal, J. Bretagne, and A. Laganà, *Chem. Phys.* **117**, 177 (1987).
- [23] C. Gorse, M. Capitelli, J. Bretagne, and M. Bacal, *Chem. Phys.* **93**, 1 (1985).
- [24] B. Jackson and M. Persson, *J. Chem. Phys.* **96**, 2378 (1992).
- [25] M. Péalat, J. P. E. Taran, M. Bacal, and F. Hillion, *J. Chem. Phys.* **82**, 4943 (1985).
- [26] A. Laganà, in *Non-Equilibrium Processes in Partially Ionized Gases*, edited by M. Capitelli and J. N. Bardsley (Plenum, New York, 1990), p. 105.
- [27] C. Gorse, R. Celiberto, M. Cacciatore, A. Laganà, and M. Capitelli, *Chem. Phys.* **161**, 211 (1992).
- [28] C. Gorse (private communication).
- [29] A. Laganà (private communication).
- [30] J. M. Wadehra (private communication).
- [31] H. Ehrhardt, L. Langhans, F. Linder, and H. S. Taylor, *Phys. Rev.* **173**, 222 (1969).
- [32] R. Celiberto, P. Cives, M. Cacciatore, M. Capitelli, and U. T. Lamanna, *Chem. Phys. Lett.* **169**, 69 (1990).
- [33] C. F. Chan, C. F. Burrell, and W. S. Cooper, *J. Appl. Phys.* **54**, 6119 (1983).
- [34] J. R. Hiskes and A. M. Karo, *J. Appl. Phys.* **56**, 1927 (1984).
- [35] A. P. Hickman, *J. Chem. Phys.* **70**, 4872 (1979).
- [36] R. K. Janev, W. D. Langer, K. Evans, Jr., and D. E. Post, *Elementary Processes in Hydrogen-Helium Plasmas* (Springer-Verlag, Berlin, 1987), p. 231.
- [37] A. M. Bruneteau and M. Bacal, *J. Appl. Phys.* **57**, 4342 (1985).
- [38] M. Bacal, J. Bruneteau, and P. Devynck, *Rev. Sci. Instrum.* **59**, 2152 (1988).
- [39] M. Bacal, G. W. Hamilton, A. M. Bruneteau, H. J. Doucet, and J. Taillet, *Rev. Sci. Instrum.* **50**, 719 (1979).
- [40] M. Bacal, A. M. Bruneteau, W. G. Graham, G. W. Hamilton, and M. Nachman, *J. Appl. Phys.* **52**, 1247 (1981).
- [41] M. Bacal, A. M. Bruneteau, and M. Nachman, *J. Appl. Phys.* **55**, 15 (1984).